Active Rib Experiment for Adaptive Conformal Wing

by

Antony Jameson
Department of Mechanical & Aerospace Engineering
Princeton University
Princeton, New Jersey 08544

and

F. Austin, M.J. Rossi,, W. VanNostrand and G. Knowles
Grumman Corporate Research Center
Bethpage, NY 11714

Third International Conference
on Adaptive Structures

San Diego, CA
November 1992

Active Rib Experiment for Adaptive Conformal Wing

by

**Fred Austin,* Michael J. Rossi,* Antony Jameson,†
William Van Nostrand,* Joseph Su,* and Gareth Knowles***

ABSTRACT

Optimum wing cross-sectional profiles were developed for two transonic cruise conditions. It is shown that significant reductions to the shock-induced drag can be achieved by maintaining the optimum shape during transonic cruise as the flight condition changes. Only small, potentially achievable, adaptive modifications to the profile are required. A general method was developed to adaptively deform structures to desired shapes, and the method is employed to achieve commanded wing rib shapes. The method was investigated by a finite-element analysis of an adaptive rib and by experimental investigations on a rib model. Open-loop experiments of the unloaded structure show that commanded shapes can be achieved.

INTRODUCTION

Potential applications of adaptive structures for improving aerodynamic and/or hydrodynamic performance include rotorcraft [1], wing sections [2,3], and submersibles [4], and are implemented by attaching or embedding active materials, incorporating shape memory alloys, piezoceramics, or electrorheological devices. Variable camber has been studied to reduce the critical root bending moment, to reduce drag, and to improve gust-alleviating response [5]. Unlike that study as well as the AFTI/F-111 investigation [3], which addressed the advantages of adaptively modifying the wing leading and trailing edges to achieve relatively large deformations, we are concentrating on the use of adaptive wings to improve aircraft performance during transonic cruise, a problem that requires smaller shape changes, but primarily in the region between the leading and trailing edges. By finding an improved design for subsonic loiter, we previously reported that it is possible to reduce the drag coefficient of the USAF E-8C JSTARS aircraft by at least 6%, while maintaining efficient performance during cruise [6]. However, we now find that far more dramatic performance improvements can be achieved for a fighter aircraft in the transonic region.

During transonic cruise, the air accelerates to supersonic speeds over portions of the wing, and a shock, inducing significant drag, usually occurs; however, this drag can be reduced dramatically if the airfoil has the correct shape. Wings that are optimized for a single cruise condition, therefore, usually have high drag at other cruise conditions. However, by adaptively modifying the wing cross section, it is possible to maintain optimum performance as the flight condition changes.

* Grumman Corporate Research Center, Bethpage, NY 11714

† Princeton University, Olden St., Engineering Quadrangle, Princeton, NJ 08544

Presented at the Third International Conference on Adaptive Structures, San Diego, Nov. 1992

AERODYNAMIC ANALYSIS

In order to assess the potential payoff from a variable wing structure, it is necessary to identify the critical operating conditions where shape modifications might significantly improve the aerodynamic performance, and the range of shape variations that might be needed. During the last several years, Jameson [7,8] has investigated the feasibility of using control theory to formulate the problem of optimum aerodynamic design. This has led to a new design method which merges concepts and techniques from computational fluid dynamics and control theory.

The key ideas are as follows. Suppose that the performance is measured by a cost function I. For example, to optimize a wing section one might take

$$I = \alpha_1 \int_S (p - p_D)^2 \, dS + \alpha_2 C_D \tag{1}$$

where p is the surface pressure, p_D the desired surface pressure, and the integral is over the surface, while C_D is the drag coefficient and α_1 and α_2 are weights. Suppose now that the shape is defined by a function $f(x)$. Then one wishes to calculate the gradient or Frechet derivative $g = \partial I / \partial f$, such that if a change δf is made in f, then the first order change in I is $\delta I = \int_S g \, \delta f \, dS$. If one sets $\delta f = -\lambda g$ where λ is sufficiently small and non-negative, then

$$\delta I = -\int \lambda g^2 dS < 0 \tag{2}$$

so an improvement is guaranteed unless $g = 0$, which is the condition for an optimum. Although g is the derivative in function space of an infinite-dimensional vector f, as shown in [8], it can be calculated indirectly by solving an adjoint problem, at a cost about equal to that of a flow situation. Thus, successive improvements towards the optimum can be made with iterations, each of which has a computational cost of about two flow solutions.

This method has been implemented with the transonic potential flow equation [8] and was used in the present study to develop optimum wing sections for a fighter aircraft at different design points. The simplification that results from the use of the nonlinear potential flow model makes it possible to perform the design calculations rapidly enough to allow a range of alternatives to be examined. Each calculation can be performed about 10 minutes on an IBM RS 6000 model 530 workstation. To check the validity of the results, the performance of each design was then evaluated by calculating the solution of the Euler equations for a range of transonic conditions.

A hypothetical fixed-wing version of the F-14 aircraft was selected as an example for this study. The choice of representative design points for the wing section is complicated by the fact that the actual F-14 wing has variable sweepback which is normally adjusted to keep the effective Mach number and angle of attack in a range within which the existing section is quite efficient. An examination of the currently used program for sweep variation indicated that the most likely opportunity for improvement is in the transonic regime with the aircraft operating at a high subsonic Mach number with high lift and low sweep. A representative cruise condition is Mach .73 at 28° sweep with a lift coefficient $C_L = .65$. According to the simple theory of sweepback for a wing of infinite span, these are equivalent to a two-dimensional condition of Mach .69 with $C_L = .85$. This was taken as one design point, labeled "Y" in the study. The existing section already has a significant shock-induced drag of 39 counts ($C_D = .0039$) in this condition.

The design method was used to try to minimize C_D at the design point, while simultaneously minimizing the change in the subsonic pressure distribution at Mach .2 in order to make the shape changes as small as possible. To prevent the design method from producing sections which are undesirably thin, an additional penalty for reduction of the contained volume was included in the cost function. Also, the initial section from which the optimization was

started was thickened. In this way a number of sections of varying thicknesses were obtained, these being labeled F-14Y, F-14YT, F-14YU, and F-14YV in ascending order of thickness. Euler calculations verify that the shock-induced drag can be reduced to 5 to 7 counts at the design point, while the thickness may also be slightly increased.

To examine the influence of modifications in the design point, a second point "X" was then selected with a slightly higher Mach number and lower lift coefficient, Mach .72 and $C_L = .75$. The same optimization procedure was used to produce another sequence of designs F-14X, F-14XT, F-14XU, and F-14XV, again in ascending order of thickness. The existing F-14 section has a shock-induced drag coefficient of 75 counts in this condition. Again it was verified with Euler calculations that the shock-induced drag could be reduced to 7 to 10 counts without reducing the thickness.

Key results are shown in Table I. The four airfoils beginning with the designation F-14X have been optimized for the X design point, and the four airfoils beginning with the designation F-14Y have been optimized for the Y design point. The drag is shown at the design point for which the airfoil has been optimized as well as for the other design point. For each of these optimum airfoils, it is seen that the drag is significantly higher at the off-design point and is reduced to moderate levels at the design point. The airfoils in each series can be potentially modified from one to the other by adaptive control; i.e. the F-14X airfoil can be modified into the F-14Y airfoil, the F-14XT airfoil can be modified into the F-14YT airfoil, etc. The most desirable pair seemed to be the F-14XU and F-14YU since they are slightly thicker than the existing F-14 section and have approximately the same drag as the thinner F-14X and F-14Y airfoils. Additional thickness might be used to advantage to reduce structure weight or to increase the wing span, which reduces the drag induced due to lift. As shown in Figure 1, the required shape changes for each of the four series (nominal, thick, thicker, and thickest) are small and are, therefore, potentially achievable. Consequently, it appears possible that as flight conditions change, adaptive variation of the wing cross section could enable the optimum section to be used continuously to dramatically reduce the shock-induced drag thereby extending the transonic cruise envelope.

STRUCTURAL ANALYSIS AND DEVELOPMENT OF GAIN MATRICES

The method developed below is general and can be applied to other types of problems to achieve adaptive changes to structural shapes. As indicated in Figure 2, our design employs active trusses that form the wing ribs. The diagonal elements are linear actuators that expand

TABLE I – SHOCK-INDUCED DRAG

DESIGN POINT X M = .72, C_L = .75
DESIGN POINT Y M = .69, C_L = .85

AIRFOIL		C_D	
DESIGNATION	SERIES	POINT X	POINT Y
F-14X	NOMINAL	.0007	.0033*
F-14XT	THICK	.0010	.0032*
F-14XU	THICKER	.0007	.0034*
F-14XV	THICKEST	.0008	.0036*
F-14Y	NOMINAL	.0068*	.0006
F-14YT	THICK	.0061*	.0005
F-14YU	THICKER	.0041*	.0006
F-14YV	THICKEST	.0037*	.0007

*Off-design condition

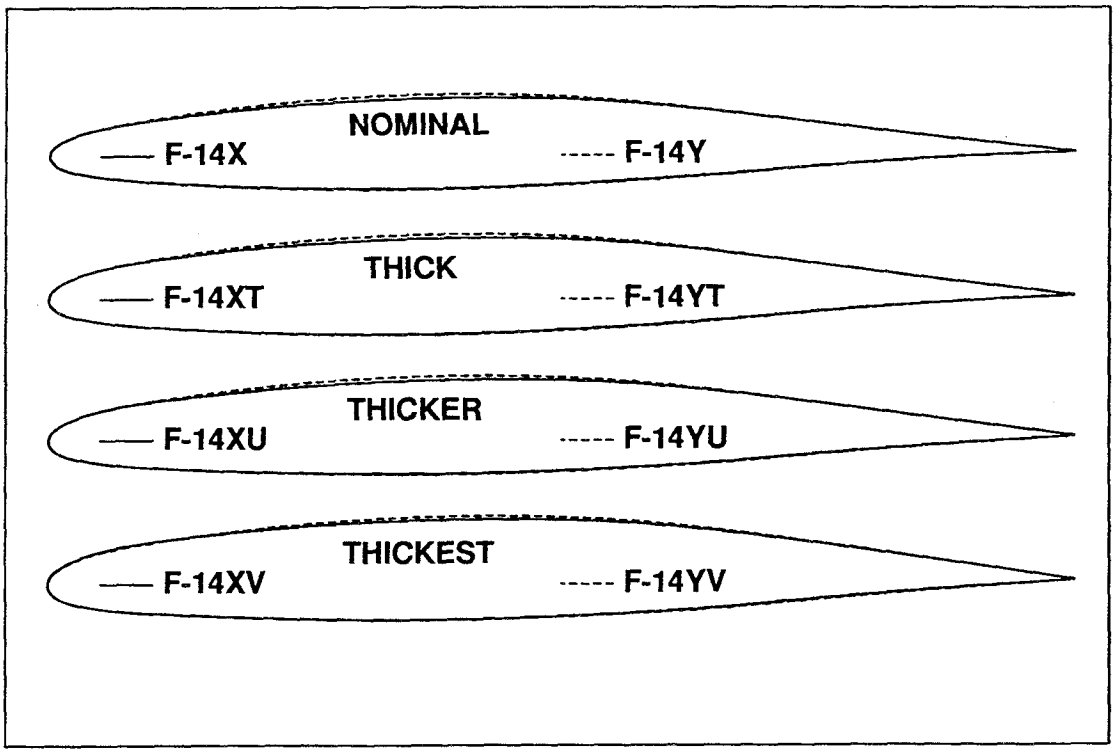

Figure 1 Optimum Wing Cross Sections for Two Design Points

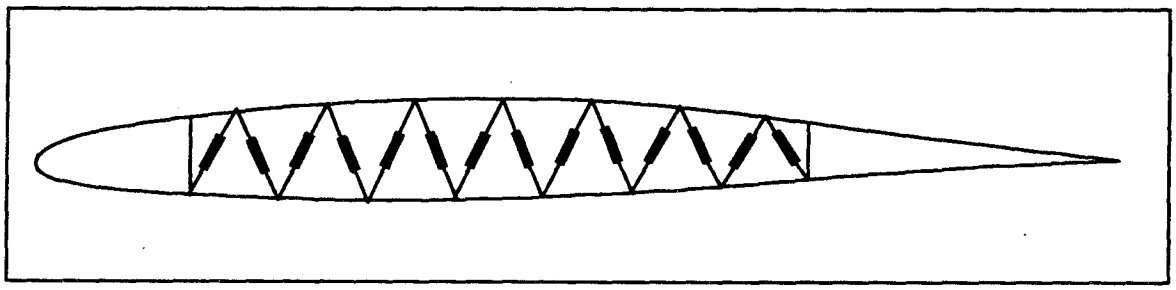

Figure 2 Use of Adaptive Truss for Wing Rib

and contract to deform the airfoil. The variables used in the structural analysis and their coordinate systems are shown in Figure 3. **x** and **f** are the deformations and forces on the structure, respectively, in the global coordinate system. A finite-element model of the structure, without the actuators, is developed to obtain the system stiffness matrix **K**. The actuators are represented by the loads that they exert on the structure. The structural equations are

$$\mathbf{f}_a + \mathbf{f}_e = \mathbf{K}\mathbf{x} \tag{3}$$

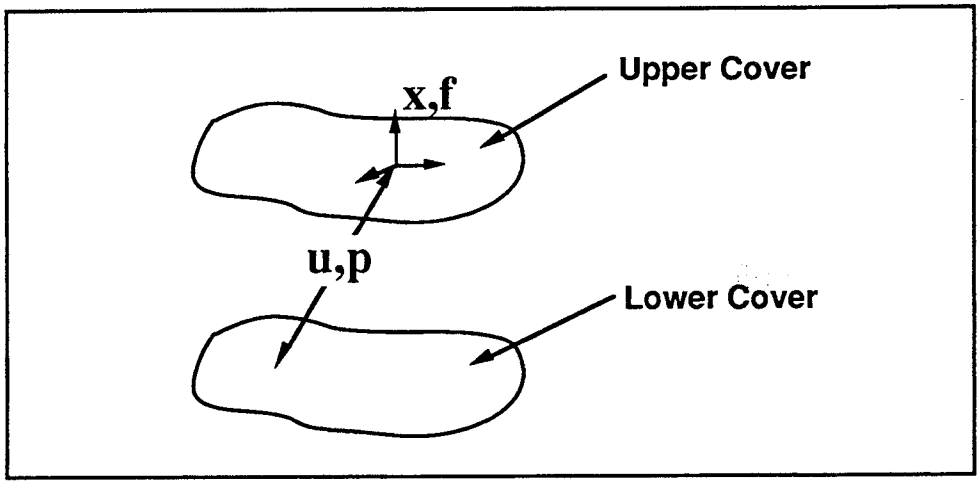

Figure 3 General Structure with Global and Actuator Coordinate Systems

where $\mathbf{f_a}$ is a vector of the actuator loads in global coordinates and $\mathbf{f_e}$ is a vector of aerodynamic and, possibly, other external loads. It is assumed that $\mathbf{K}$ is nonsingular so that we can write

$$\mathbf{x} = \mathbf{A}(\mathbf{f_a} + \mathbf{f_e}) \tag{4}$$

where $\mathbf{A} = \mathbf{K}^{-1}$.

The problem is to compute the actuator displacements or loads while specifying only some of the elements of $\mathbf{x}$, such as selected displacements normal to a wing surface, to describe the desired shape. If $\mathbf{p}$ is a vector of the actuator loads along the actuators, taken as positive when the actuators are in compression and pushing against the structure, then

$$\mathbf{f_a} = \mathbf{Tp} \tag{5}$$

where $\mathbf{T}$ contains the direction cosines of the actuator loads as well as information specifying that the actuator loads are applied to the structure in equal and opposite pairs. Since virtual work is conserved,

$$\mathbf{u} = \mathbf{T}^{\mathrm{T}}\mathbf{x} \tag{6}$$

where $\mathbf{u}$ is a vector containing the extensions of each actuator. Equations (4), (5), and (6) are combined to obtain

$$\mathbf{u} = \mathbf{A_p p} + \mathbf{T}^{\mathrm{T}}\mathbf{A f_e} \tag{7}$$

or

$$\mathbf{p} = \mathbf{K_p}\left(\mathbf{u} - \mathbf{T}^{\mathrm{T}}\mathbf{A f_e}\right) \tag{8}$$

where $\mathbf{A_p} = \mathbf{T}^{\mathrm{T}}\mathbf{AT}$ and $\mathbf{K_p} = \mathbf{A_p}^{-1}$. By combining Eqs. (4), (5), and (8),

$$\mathbf{x} = \mathbf{B}\mathbf{u} + \left(\mathbf{A} - \mathbf{B}\mathbf{T}^{\mathrm{T}}\mathbf{A}\right)\mathbf{f}_{\mathbf{e}} \tag{9}$$

where $\mathbf{B} = \mathbf{A}\mathbf{T}\mathbf{K}_{\mathbf{p}}$.

MINIMUM ACTUATOR DISPLACEMENTS

The control laws can be developed either by minimizing the actuator displacements or the actuator loads. In this subsection, we describe the procedure to minimize actuator displacements.

If $\mathbf{x}_1$ contains only those elements of $\mathbf{x}$ whose deflections are desired specified quantities, Eq. (9) yields

$$\mathbf{x}_1 = \mathbf{B}_1\mathbf{u} + (\mathbf{A}_1 - \mathbf{B}_1\mathbf{T}^{\mathrm{T}}\mathbf{A})\mathbf{f}_{\mathbf{e}} + \mathbf{r}_{\mathbf{x}} \tag{10}$$

where the subscript 1 indicates that all rows of the corresponding matrix are deleted except those corresponding to the elements of $\mathbf{x}_1$, and $\mathbf{r}_{\mathbf{x}}$ is an error residual vector which is nonzero if this equation cannot be satisfied exactly. Then,

$$\mathbf{u} = (\mathbf{B}_1)^{\dagger}\left[\mathbf{x}_1 - \left(\mathbf{A}_1 - \mathbf{B}_1\mathbf{T}^{\mathrm{T}}\mathbf{A}\right)\mathbf{f}_{\mathbf{e}}\right] \tag{11}$$

where the dagger indicates the Moore-Penrose pseudo-inverse (of $\mathbf{B}_1$) which has the following properties [9]: The solution provides the best fit solution to Eq. (11) in the sense that $\|\mathbf{r}_{\mathbf{x}}\|$, the 2-norm of the error residual, is minimized, and, when the solution is not unique, Eq. (11) provides the solution that minimizes $\|\mathbf{u}\|$. In practice, this means that if more deflections (components of $\mathbf{x}_1$) are specified than the number of actuators (components of $\mathbf{u}$), Eq. (11) will provide the actuator displacements that are a best (least square) fit to Eq. (10). If there are fewer specified deflections than actuators, or if $\mathbf{B}_1$ is rank deficient, an infinite number of solutions $\mathbf{u}$ are possible, and the solution that is obtained is the one that minimizes the actuator deflections.

From Eq. (11),

$$\mathbf{u}_{\mathbf{d}} - \mathbf{u} = (\mathbf{B}_1)^{\dagger}(\mathbf{x}_{1\mathbf{d}} - \mathbf{x}_1) \tag{12}$$

where $\mathbf{u}_{\mathbf{d}}$ and $\mathbf{x}_{1\mathbf{d}}$ contain the desired values and $\mathbf{u}$ and $\mathbf{x}_1$ contain the current values. Thus $(\mathbf{B}_1)^{\dagger}$ may be used as a gain matrix when controlling actuator displacements to achieve the desired structural deformations with minimum actuator strokes.

To obtain minimum actuator deflections by controlling actuator loads, Eq. (11) is substituted into Eq. (8), and a similar analysis reveals that

$$\mathbf{p}_{\mathbf{d}} - \mathbf{p} = \mathbf{K}_{\mathbf{p}}(\mathbf{B}_1)^{\dagger}(\mathbf{x}_{1\mathbf{d}} - \mathbf{x}_1) \tag{13}$$

Thus $\mathbf{K}_{\mathbf{p}}(\mathbf{B}_1)^{\dagger}$ is the gain matrix when controlling actuator loads to achieve the desired structural deformations with minimum actuator displacements.

MINIMUM ACTUATOR LOADS

We substitute Eq. (5) into Eq. (4) and delete equations corresponding to coordinates that are not desired specified deformations to obtain

$$\mathbf{x}_1 = \mathbf{A}_1(\mathbf{T}\mathbf{p} + \mathbf{f}_e) + \mathbf{r}_p \tag{14}$$

where $\mathbf{r}_p$ is the residual vector. This equation is solved for $\mathbf{p}$, and the result is

$$\mathbf{p} = (\mathbf{A}_1\mathbf{T})^{\dagger}(\mathbf{x}_1 - \mathbf{A}_1\mathbf{f}_e) \tag{15}$$

If there are more specified deflections than actuators, Eq. (15) yields the value of $\mathbf{p}$ that provides the best-fit solution to Eq. (14). If there are more actuators than specified deflections, there are an infinite number of solutions to Eq. (14), and Eq. (15) provides the solution that minimizes the norm $\|\mathbf{p}\|$. Equation (15) is substituted into Eq. (7), and the result is

$$\mathbf{u} = \mathbf{A}_p(\mathbf{A}_1\mathbf{T})^{\dagger}\mathbf{x}_1 + [\mathbf{T}^{\mathrm{T}}\mathbf{A} - \mathbf{A}_p(\mathbf{A}_1\mathbf{T})^{\dagger}\mathbf{A}_1]\mathbf{f}_e \tag{16}$$

By using the same reasoning as was used in the previous section, to achieve desired structural deflections with minimum actuator loads, the gain matrices to control actuator loads and actuator displacements are $(\mathbf{A}_1\mathbf{T})^{\dagger}$ and $\mathbf{A}_p(\mathbf{A}_1\mathbf{T})^{\dagger}$, respectively.

TEST ARTICLE

We constructed a model of an adaptive rib with 14 actuators to demonstrate the concept (Figures 4 and 5). The model is approximately 4 ft wide and 10 in high. The upper and lower caps are aluminum with T-shaped cross-sections (3 in wide, .050 in thick, with .50 in by .25 in ribs). In the undeformed condition, the upper and lower surfaces are flat. Fourteen actuators are used to form the truss structure. Terfenol-based magnetostrictive actuators being developed by NSWC/WO have the potential to meet the load requirements while being light in weight; however, since they are not yet available, in our model mechanical ball-screw actuators are used.

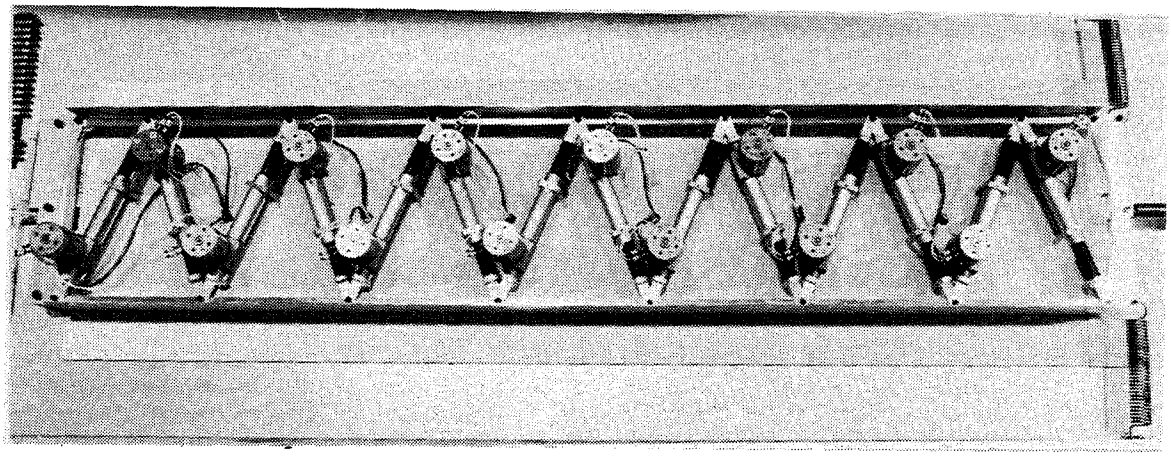

Figure 4 Adaptive Rib Test Article

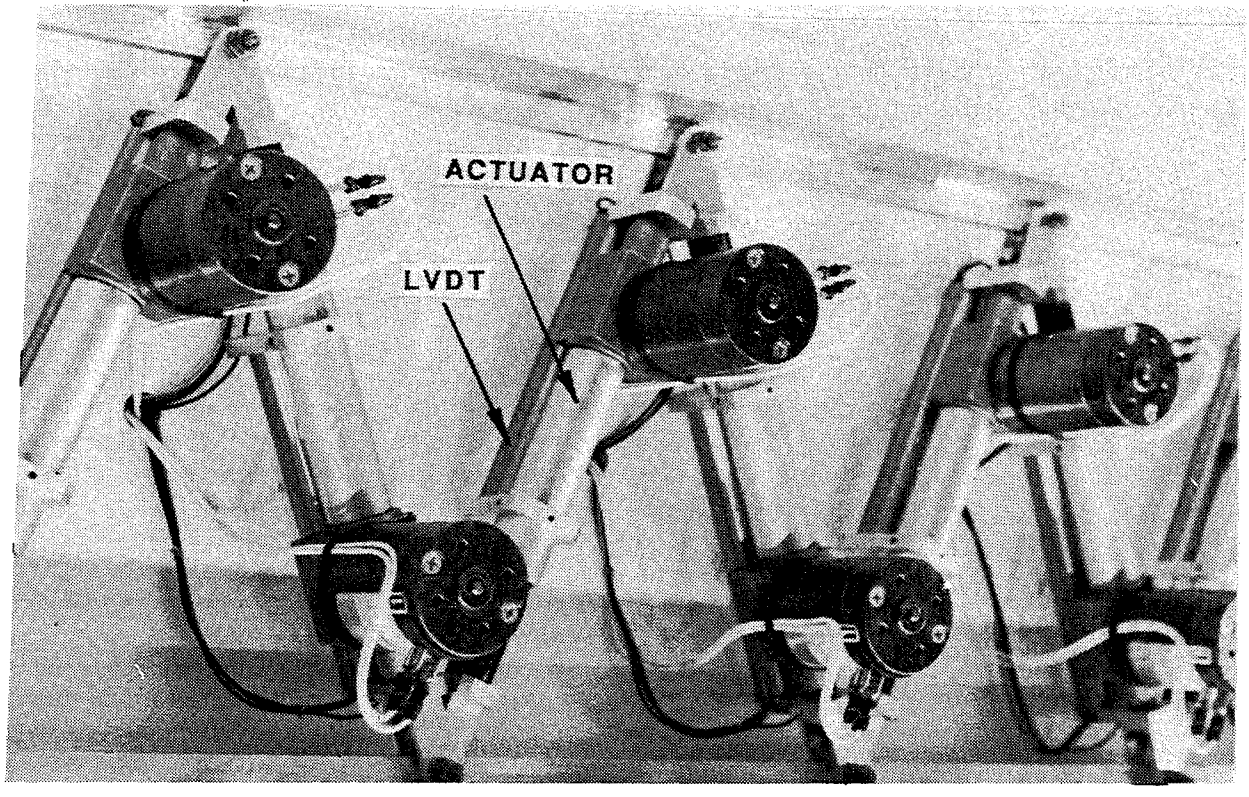

Figure 5 Detail of Actuators and LVDTs

FINITE-ELEMENT ANALYSIS

A finite-element (FE) model, containing 206 beam elements and 30 triangular-membrane elements (Figure 6), was used to obtain the loads needed to achieve various rib shapes as computed by applying the above method with the Grumman COMAP ASTRAL FE system. The structure is pin-connected at points A and B and spring-connected to ground at point C in the x, y , and θ directions to represent spar flexibility. Some of the deformed shapes obtained are illustrated in Figure 7. In each case, the curved surface is a half sinusoid. The deflection normal to the surface was specified at 14 points, and since there are 14 actuators, we were able to achieve the deflections at those points exactly, when the actuator loads **p** were applied in the FE analysis. The bottom-surface deflections in Figures 7b and c, at first, seem counter-intuitive since the loads in the actuators must be equal and opposite and the surfaces do not deform in opposing directions; however, it is easy to verify that the loads applied to each vertex by adjacent actuators can combine such that zero or net upward loads occur at each lower vertex, while net upward loads occur at each upper vertex, with equal and opposite loads in each actuator. Racking (Figure 7d) is one method of achieving wing twist.

CONTROL SYSTEM

A nonlinear finite-element analysis of the model shows that, with actuator load control, nonlinear effects can produce up to 8% errors in the surface for a selected camber deformation. Consequently, actuator deflection control, which we believe will produce far more accurate deformations than load control, has been selected to achieve desired upper and lower rib-surface shapes. The control law relating actuator displacements to the desired shape was based on the theory for minimum actuator displacements. However, since the 14 transverse

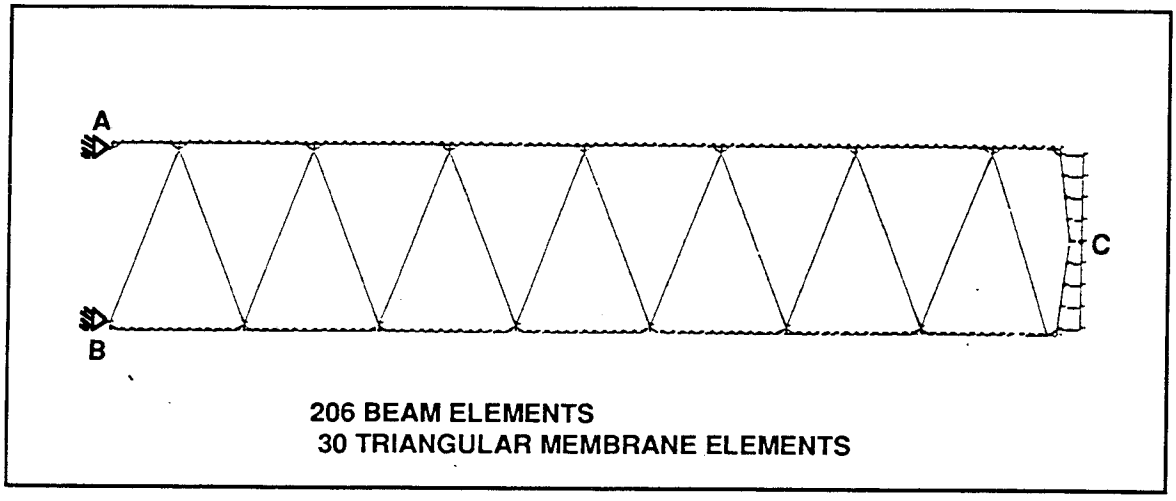

Figure 6 Finite-Element Model

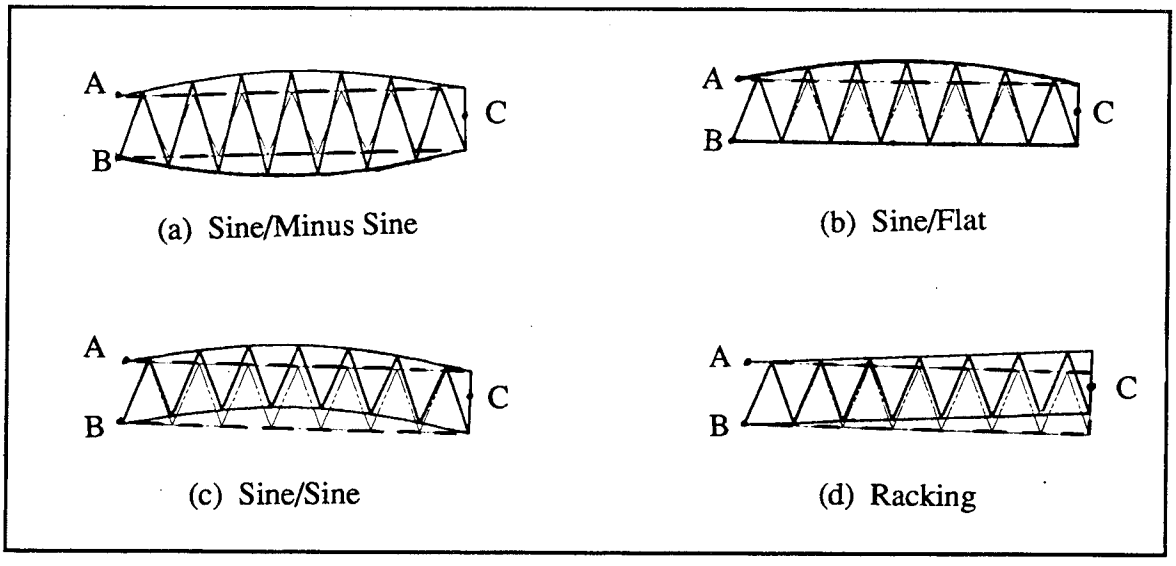

Figure 7 Deflections Achieved by Finite-Element Analysis

displacements of the movable truss hinges were selected to define the surface shapes, and there are also 14 actuators, the solution is unique; consequently, the theory to minimize actuators loads would have provided the same control matrix. A flow diagram illustrating the control concept is shown in Figure 8. Fourteen inner control loops (not shown) employ rate and velocity feedback to control each actuator so that it achieves its commanded actuator deflection.

COMMAND, CONTROL, AND MEASUREMENT

A command, control, and measurement computer (CCMC) was developed to command the shape of the test article experiment, to implement the control concept, and to facilitate the collection of data. A flow diagram of the concept is shown in Figure 9. The CCMC contains several plug-in boards including a Texas Instruments digital signal processing (DSP) chip

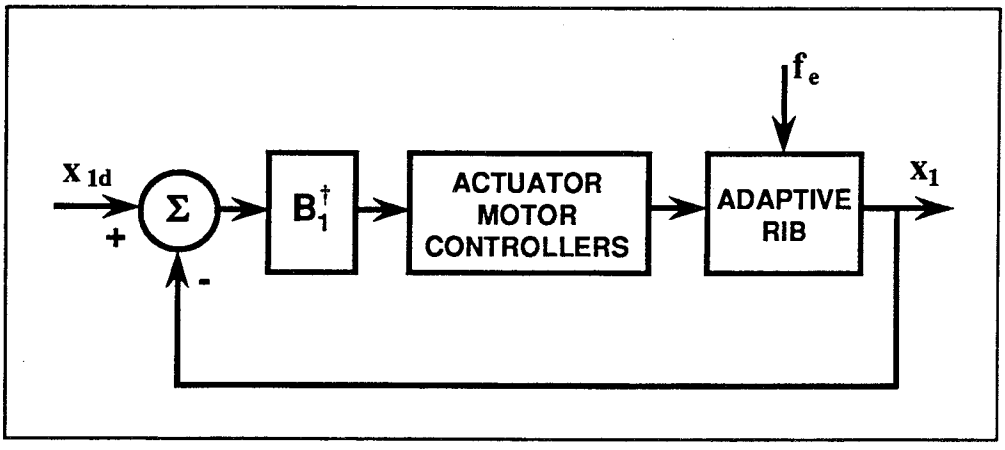

Figure 8 Flow Diagram of Control System

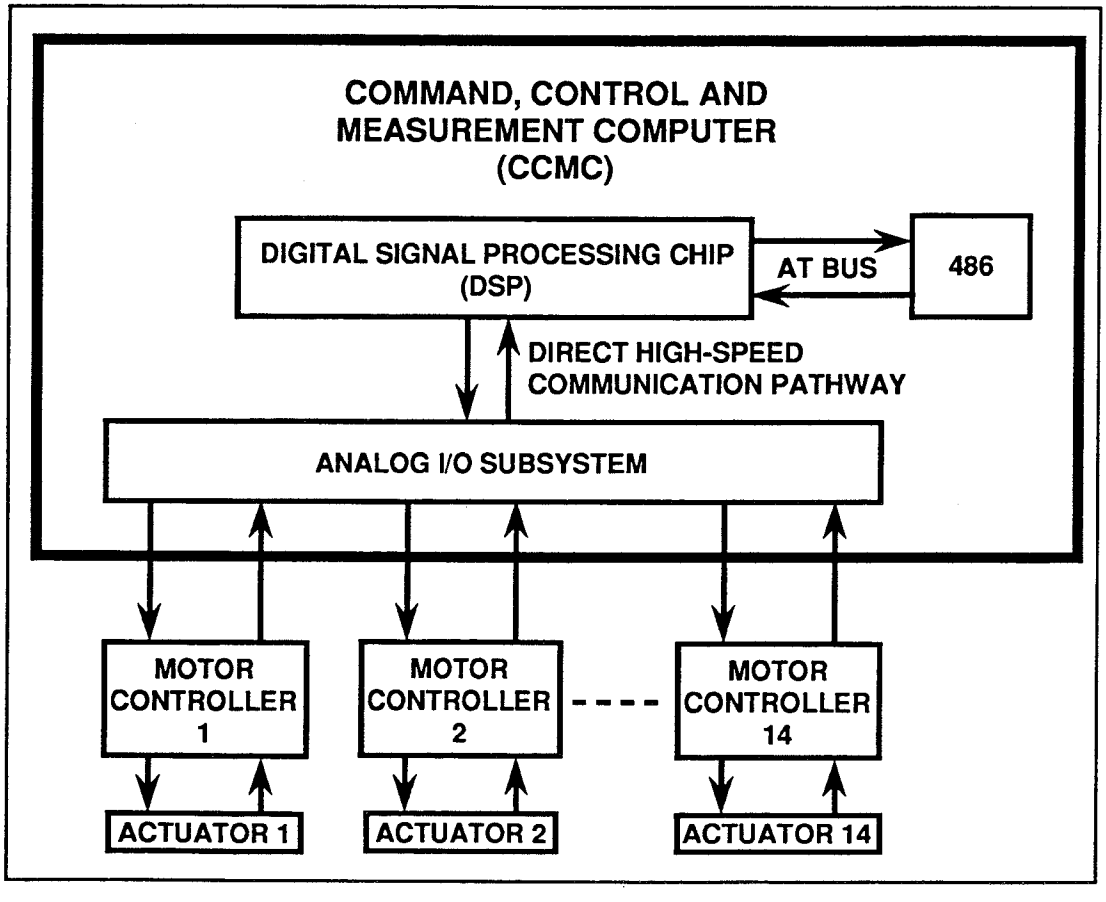

Figure 9 Command, Control, and Measurement System Architecture

which is connected to a 486 microprocessor with an AT bus. Seventeen MB of memory enables recording time history data of deflection, force, cover deformation, and commanded voltage at a rate of up to 100 Hz. User commanded shapes are entered in the 486 and are communicated to the DSP for processing. To limit the dynamic response, the shape changes are gradually applied over a 5-sec period according to a one minus cosine waveform. The desired stroke of each actuator is computed and relayed to its motor controller; a direct high-speed communication pathway and an Analog I/O Subsystem perform this task. Each motor controller incorporates analog position error feedback and motor speed regulation to achieve the commanded actuator stroke. The motor controllers employ pulse-width modulation of a 20 KHz sinusoidal wave to regulate the motors. Thus, the controllers act as linear amplifiers. The hierarchical control system architecture allows the CCMC to augment the loop gain provided by the motor-controller analog position error feedback to reduce stiction, thereby improving the regulator accuracy.

An LVDT is located in parallel to each actuator to sense its deflection (Figure 5). The rib shape will be sensed by a second set of LVDTs (not shown) that are externally attached to the upper and lower surfaces. As an alternative method of measuring surface deflections, we are also planning to install an optical CCD system. This system is being developed at Polytechnic University by Mr. Zhong-Ziang Zuang under the direction of Prof. Farshad Khorramy and is capable of simultaneously measuring the positions of sixteen bright spots located on the upper- and lower-rib surfaces. These positions are obtained in digital form, and are communicated to the CCMC at a rate of 30 times per second. The mechanism for accomplishing this is based on feeding the output of a conventional monochrome CCD video camera to a custom PC board where a threshholding algorithm transforms the signal to digital position data. Fourteen of the data points correspond to surface points adjacent to the 14 movable hinges of the truss, while the remaining two are fixed reference positions on the structure.

A stress-ratio matrix was developed to predict whether any commanded deformation will result in stresses that are beyond safe allowable values (ultimate stresses with safety factors of 2). When this matrix is multiplied by the vector specifying the desired shape $\mathbf{x}_1$, it provides the ratio of the stresses in each finite element to their allowable values. The matrix resides in the DSP, and the stress computations are performed in real time. If a shape command will result in a stress that is beyond the safe value, the command is automatically scaled down and the operator receives an indication. Also, if unpredicted actuator deflections cause stresses that exceed the allowable safe values, the experiment is automatically shut down This stress monitoring is accomplished at rates of up to 100 times per second by measuring the actuator strokes and communicating them to the DSP where the stress ratios are computed. The automatic shut-down is implemented by sending a disable signal to all of the motor controllers to stop all further actuation.

In addition to these safety features, the forces and deflections are limited for each actuator. The force and deflection limits differ for each actuator according to its requirements. The maximum working range of deflection is ± 1 in and of force is ± 100 lbs. Upper and lower deflection limits are achieved by adjusting the saturation in the preamplifier in each motor controller. Adjustable current limits in the controllers are used to limit the output torques to the motors and thereby limit the output forces of the actuators.

TEST RESULTS

Neither the external LVDT or the noncontacting CCD optical system described in the previous section has been installed to date; therefore, the results that will be presented are with the loop opened in Figure 8. (However, the internal LVDTs that parallel each actuator were used and the loops were closed in each of the 14 separate actuator control systems). Figure 10

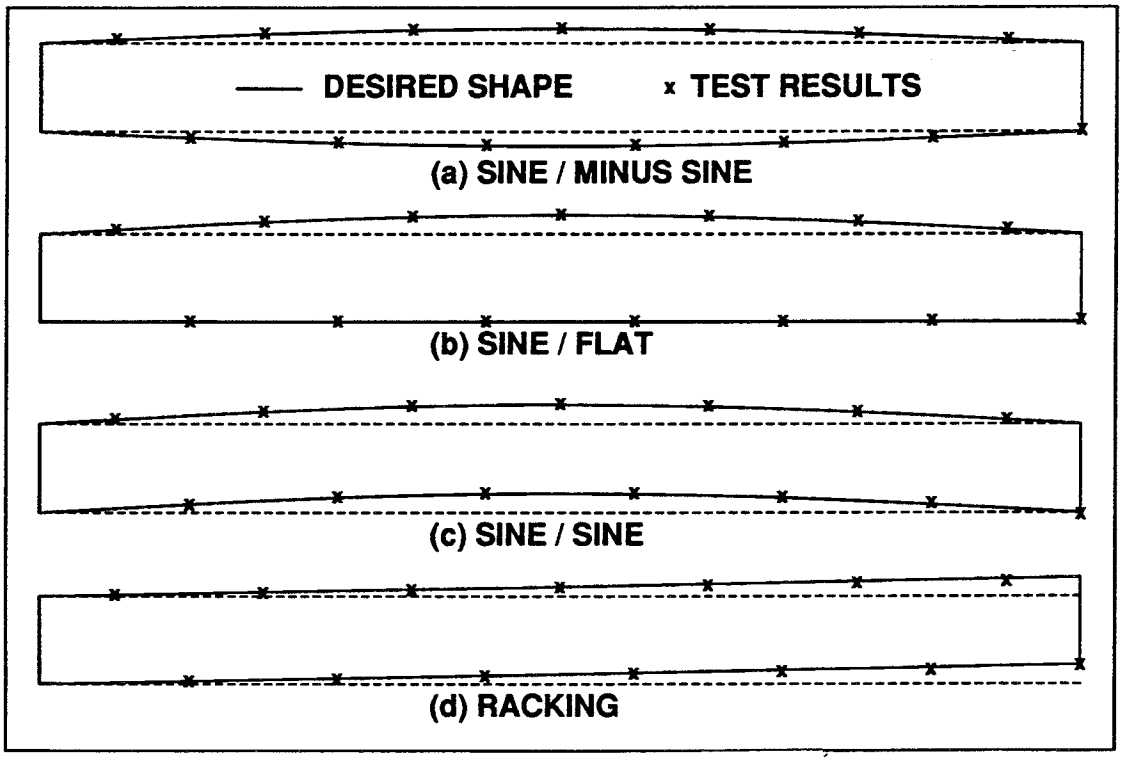

Figure 10 Test Results

shows the test measurements superimposed on the desired shapes. Each shape corresponds to one of the shapes that were studied by finite-element analysis (Figure 7). No external loads were applied in these tests since overall loop closure is required to obtain desired shapes for the loaded structure. Each actuator-LVDT assembly was calibrated to an accuracy of ±.01 in. Surface errors are small for each of the first three shapes. Somewhat larger errors occur for the racking condition. Since the magnitudes of all of the required actuator strokes are lower than .07 in for this condition, calibration errors and stiction have a much larger effect on racking. All errors are expected to be reduced significantly when the overall system loop is closed.

CONCLUSIONS

For the transonic flight conditions investigated, wing drag was reduced from values of 32 to 68 counts to 5 to 10 counts, by small adaptive changes in the wing cross-sectional shape. An analytical method to achieve the shape changes has been developed. This method is general and can be applied to other shape-control problems. A model of an adaptive rib has been constructed, and finite-element analysis of the model verifies that the method can provide a close fit to any desired shape change that does not over-stress the structure. A computer was developed to provide the command, control, and measurement functions. Commanded shapes were achieved during open-loop control experiments of the unloaded structure. Closed-loop experiments with simulated aerodynamic loads are recommended.

ACKNOWLEDGMENTS

The authors gratefully acknowledge the contributions of Christopher C. Tung for finite-element studies, Edward Sheedy for mechanical and structural design, Paul V. Aidala and Walter G. Jung for advice on practical aerodynamic considerations, Martin Kesselman for

electronic design and analysis, Norman Peele for electrical circuit design and assembly, and Ronald L. Heuer for advice on design and manufacturing.

REFERENCES

1. Chopra, I., et al., 1991. Proc. Army Research Office Workshop on Rotorcraft Technology.

2. MacLean, B. J., Carpenter, B. F., Draper, J. L., Misra, M. S., Nov. 1991. "A Compliant Wing Section for Adaptive Control Surfaces." Proc. Conf. on Adaptive Materials and Active Structures, Alexandra, Virginia.

3. Bonnema K. L., and Lokos, W. L., April-May 1989. "AFTI/F-111 Mission Adaptive Wing Flight Test Instrumentation Overview." 35th International Symposium of the Instrumentation Society of America."

4. Beauchamp, C. H., Nadolink, R. H., Dickinson, S. C., and Dean, L. M., May 1992. "Shape Memory Alloy Adjustable Camber (SMAAC) Control Surfaces." First European Conference on Smart Structures, Glasgow, Scotland.

5. Spillman, J. J., January 1992. "The Use of Variable Camber to Reduce Drag. Weight and Costs of Transport Aircraft." Aeronautical Journal, 1-9.

6. Austin, F, Knowles, G. J., Jung, W. G., Tung, C. C., and Sheedy, E. M., May 1992. "Adaptive/Conformal Wing Design for Future Aircraft." First European Conference on Smart Structures, Glasgow, Scotland.

7. Jameson, A., Nov. 1988. "Aerodynamic Design Via Control Theory." Princeton University Report MAE 1824, ICASE Report No. 88-64, also 1988, J. of Scientific Computing, 2: 233-260.

8. Jameson, A., Feb. 1990. "Automatic Design of Transonic Airfoils to Reduce Shock Induced Pressure Drag." Princeton University Report MAE 1881, Proceedings of the 31st Israel Annual Conference on Aviation and Aeronautics, Tel Aviv, pp. 5-17.

9. Stewart, G. W, 1973. Introduction to Matrix Computations , Academic Press, San Diego, pp. 317-325.